Torque and Voltage Quality in Design Optimization of Low-Cost Non-Overlap Single Layer Winding Permanent Magnet Wind Generator

Johannes H. J. Potgieter, *Student Member, IEEE*, and Maarten J. Kamper, *Senior Member, IEEE*

***Abstract*—The main focus of this paper is cost-effective techniques to reduce the cogging torque in permanent magnet (PM) wind generators. However, there are also certain limits with which other machine design aspects need to comply. These aspects include ease of manufacturing, mass, load torque ripple, and voltage quality. In this paper, a low-cost single layer PM wind generator with an irregular, parallel slotted stator is analyzed. The sensitivity of average torque and cogging torque to machine dimension variations is investigated, as well as the effects imposed upon the load torque ripple and the voltage quality. Methods are proposed whereby regions of low cogging torque can be identified more quickly in the design optimization. Furthermore, an interesting observation is made regarding the effects imposed upon the cogging torque by varying the yoke heights. Finite element calculated results are validated by practical measurements on a 15-kW PM wind generator.**

***Index Terms*—Costs, design optimization, energy conversion, permanent magnet (PM) machines, power quality, sensitivity analysis, torque, vibrations, wind energy generation.**

Nomenclature

d_i	Machine inside diameter, mm.
d_o	Machine outside diameter, mm.
h_m	Magnet height, mm.
h_r	Rotor yoke height, mm.
h_s	Stator yoke height, mm.
k	Harmonic index.
l	Axial length of stack, mm.
p	Number of poles.
P_{cu}	Machine winding losses, W.
S	Number of stator slots.
T_{ave}	Average torque, Nm.
T_{rated}	Rated machine torque, Nm.
$\mathbf{U}$	Optimization output parameter vector.
V_1	Per phase voltage, V.
V_L	Line voltage, V.
W_s	Number of winding sections.
$\mathbf{X}_1$	Optimization input parameter vector 1.
$\mathbf{X}_2$	Optimization input parameter vector 2.
ΔT_{cog}	Peak-to-peak no-load cogging torque, Nm.
ΔT_L	Peak-to-peak load torque ripple, Nm.
$\Delta\tau$	Per unit no-load cogging torque, pu.
$\Delta\tau_L$	Per unit load torque ripple, pu.
θ_e	Electrical rotor position, degrees.
θ_M	Mechanical rotor position, degrees.
θ_g	Slot width, rad.
θ_m	Magnet pitch, rad.
θ_p	Average pole pitch, rad.
θ_S	Average slot pitch, rad.
θ_t	Slot pitch, rad.
σ_g	Slot width to average slot pitch ratio, pu.
σ_m	Magnet pitch to pole pitch ratio, pu.
σ_t	Slot pitch to average slot pitch ratio, pu.
τ_{ave}	Per unit average torque, pu.

Manuscript received December 17, 2010; revised May 10, 2011; accepted May 16, 2011. Date of publication June 16, 2011; date of current version February 3, 2012. This work was supported in part by the National Research Foundation (NRF) of South Africa.

The authors are with the Department of Electrical and Electronic Engineering, University of Stellenbosch, Stellenbosch 7600, South Africa (e-mail: kamper@sun.ac.za).

Color versions of one or more of the figures in this paper are available online at http://ieeexplore.ieee.org.

Digital Object Identifier 10.1109/TIE.2011.2159955

I. Introduction

TORQUE quality and cost are two of the most important aspects to consider in the design of direct-drive permanent magnet (PM) wind generators. Although an absolute minimum for both these aspects are essential, other factors namely, mass, efficiency, average torque performance, load torque ripple, and voltage quality cannot be excluded from the design optimization process.

Torque quality refers to the torque ripple generated by the machine, which is mainly caused by stator winding MMF-harmonics and the slotted air gap of the machine. At no-load, the slotted air gap causes the so-called cogging torque. Torque ripple can be a source of serious vibration and acoustic noise in PM wind generator systems. Moreover, cogging torque can lead to complete failure of start-up as the wind turbine generates very low torque at low turbine speeds. Thus, improving the torque quality of the PM generator to the lowest percentage torque ripple is of utmost importance.

The torque quality of electrical machines is a topic that has received and still receives extensive attention in literature. Several techniques exist to reduce the torque ripple and cogging torque by focusing on the physical properties of the electrical machine. These techniques include skewing the magnets and stator slots, varying the magnet positions, closing stator slots, and introducing auxiliary slots and teeth [1]–[9]. Manufacturing

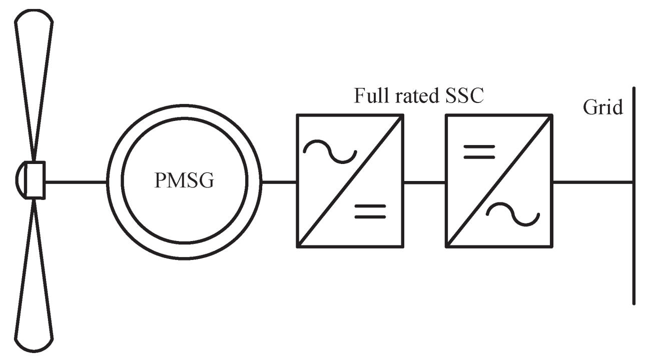

Fig. 1. Direct-drive PMSG connected to the utility grid via a full rated SSC.

and assembling tolerances in using these techniques, however, require sensitivity analysis on the dimensions of the machine [4], [9]. Furthermore, most of these techniques, due to constructional complexities, are not suitable when opting for a low-cost wind generator solution.

While the pre-mentioned techniques mainly focus on the physical properties of the PM machine, there are also certain control techniques that can be used to reduce the torque ripple in PM machines. Commonly used methods are current waveform or selected harmonic injection, direct torque control, iterative learning control, and adaptive control [10]–[19]. However, many of these techniques require an accurate knowledge of the torque characteristics of the electrical machine as well as accurate torque and speed measuring methods that can increase the cost of the machine system.

The importance of reducing the cost of manufacturing of PM wind generators can be attributed to a highly competitive market, but also to the fact that wind generator systems are still relatively expensive. An important aspect in reducing cost is to reduce the labor cost of manufacturing the machine. Furthermore, with direct-drive generators still heavier than other wind generator systems, it is, thus, essential that the mass of the PM generator be kept within reasonable limits.

The diagram of a system employing the prototype PM wind generator investigated in this study is shown in Fig. 1. The generator is directly connected to the turbine and connected to the grid via a solid-state converter or SSC. With variable speed, direct-drive systems starting to receive a significant amount of attention, the operation and control of these systems are well known as discussed in [20]–[22].

Another output performance parameter looked at in this study is the quality of the induced voltage waveform of the generator. This is particularly important if the generator is, directly connected to the grid, unlike the system layout shown in Fig. 1. There are, however, very few instances where a PM generator is directly connected to the grid in a wind generating system. Thus far, systems as such are only experimental in nature as reported in [23]–[26]. The specific prototype used in this case, however, is also proposed for future use in conjunction with the directly grid-connected system investigated in [26].

The main focus in this paper, thus, is to consider a low-cost and low cogging torque PM wind generator design. However, from most of the literature reviewed, it is evident that most of the techniques proposed are complex and can lead to an increase in the cost of the wind generator system. The design techniques for cogging torque reduction in this paper only focus on the physical properties of the machine. Furthermore, these reduction techniques are only applied to the machine design parameters without any of the more complex physical additions as proposed in most literature.

The intent, thus, is to present a more visual representation of the PM generator behavior with regard to cogging torque. The cogging effects imposed by several machine design parameters are investigated thoroughly to enable a broad interpretation of the machine cogging torque characteristics. Furthermore, the sensitivity of the PM machine to several of these machine parameters is clearly shown. This illustrates the importance of parameter selections in the correct regions with regard to parameter variations as shown in this paper.

Obviously, the average torque and efficiency performance of the PM wind generator must also be considered in the design. Furthermore, it should be ensured that the load torque ripple, voltage quality, and mass of the machine are within acceptable levels.

The aim in the design optimization, thus, is to maximize the torque output of the machine subject to minimum cogging torque. While maximization of the average torque by means of finite element (FE) analysis and optimization algorithms is no longer complex [27], the minimization of cogging torque using this process is not as easy as is shown in this paper.

II. Machine Selection and Optimization Parameters

The analysis in this paper is based on a case study of a 15-kW direct-drive PM wind generator. The generator consists of an outer rotor and inner stator with a large diameter commonly known as a “ring type” generator. The performance of this generator is at rated values of 150 r/min, 1000 Nm, 50 Hz, and 400 V. The pole number of the generator is $p = 40$. Some design detail and explanation of the PM wind generator prototype that was built and tested are given in Table I.

A. Low-Cost PM Machine Selection

With the emphasis on low cogging torque and low cost, a non-overlap winding PM machine is selected, which has lower cogging torque and also a lower number of coils than the overlap winding PM machine. To reduce labor cost, a single layer winding is chosen that has half the number of coils than the double layer winding. Further, to reduce labor cost, pre-wound coils must be used that require open and pairs of parallel stator slots.

A single layer winding also has the advantage that the slot pitch can be varied to reduce the cogging torque. A disadvantage of a single layer winding, however, is the large sub MMF harmonic that severely increases the eddy current losses in the magnets and rotor yoke if solid. Methods to reduce these losses effectively are proposed in [28]; further consideration of these losses is beyond the scope of this paper. Another possible disadvantage is the induced voltage waveform of the

TABLE I
PM WIND GENERATOR PROTOTYPE PARAMETERS

PARAMETER	VALUE	PARAMETER	VALUE
Stator inner diameter, d_i (mm)	494	Magnet material	N48H
Stator yoke height, h_s *(mm)*	10	Number of stator slots, S	48
Stator outer diameter (mm)	623	Number of turns per coil	424
Slot width, σ_g	0.44	Number of poles, p	40
Slot pitch, σ_t	1.01	Rated voltage (V)	408
Axial length of stack, ℓ (mm)	100	Rated current (A)	23
Rotor inner diameter (mm)	627	Rated output power (kW)	15
Rotor outer diameter, d_o (mm)	653.5	Rated torque (Nm)	1000
Rotor yoke height, h_r (mm)	7.25	Power factor	0.95
Rotor magnet height, h_m (mm)	6	Efficiency (%)	94.4
Magnet to pole pitch ratio, σ_m	0.73	Rated turbine speed (r/min)	150

single layer winding machine, which is known to have a high harmonic content.

With $p = 40$, there are three options of single-layer pole-slot combinations with high winding factors that can be selected for the PM wind generator. These are the 40/36, 40/42, or 40/48 combinations [29]. The 40/42 combination with only one winding section $(W_s = 1)$[30] is immediately discarded due to the unbalanced magnetic field in the air gap under load. The 40/36 combination is also a question in this regard with a very low number of winding sections namely $W_s = 2$. The 40/36 option has a lower number of coils compared to the 40/48 combination, but the ratio of the open-slot opening to the magnet pitch is larger, which is a disadvantage, and the winding factor is also lower. Another option to look at is the 42/36 combination, with the rated turbine speed then slightly lower. The slot opening to magnet pitch ratio of the 42/36 combination, however, is even worse than the 40/36 combination.

Hence, the 40/48 combination is selected with $W_s = 8$. In the FE modeling, negative boundary conditions can be used [30], and only five poles and six slots have to be meshed. A cross section of the FE model of the single-layer, open and paralleled slots, low-cost PM generator proposed in the paper is shown in Fig. 2(a). To investigate the effects caused by the irregular, parallel slotting, a comparison is done with a regular taper slotted PM machine as shown in Fig. 2(b).

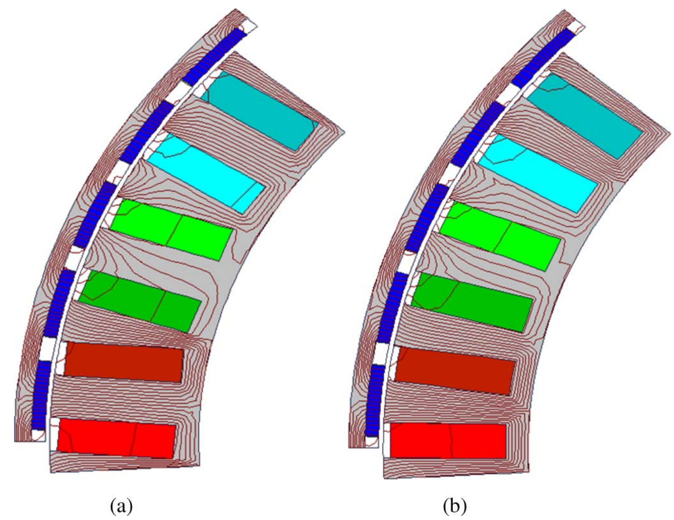

Fig. 2. (a) Irregular parallel slotted, (b) regular taper slotted PM machine sections used in the FE analysis.

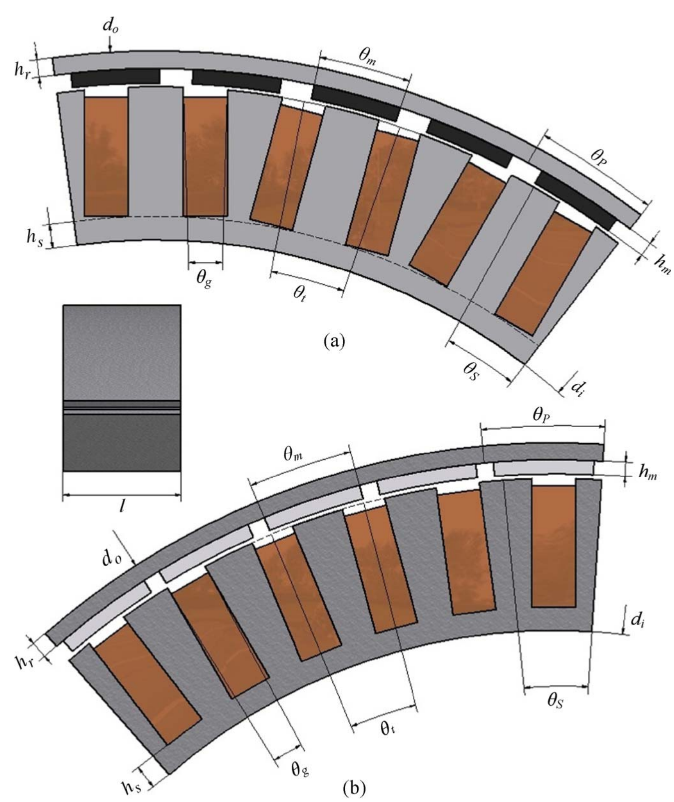

Fig. 3. Section views with parameters indicated of (a) the irregular parallel slotted, and (b) the regular taper slotted PM machines.

B. Design Optimization Parameters

The machine parameters used in the design optimization are shown in Fig. 3. The parameters that affect the cogging torque are the magnet pitch, slot pitch, the slot opening width, and the rotor and stator yoke heights. The former three dimensions are rather expressed in per unit values and are calculated as the magnet pitch to the pole pitch ratio, σ_m, the slot pitch to the average slot pitch ratio, σ_t, and the slot opening width to the average slot pitch ratio, σ_g. Mathematically, these ratios are calculated from angular dimensions as

$$\sigma_m = \frac{\theta_m}{\theta_p}; \quad \sigma_t = \frac{\theta_t}{\theta_s}; \quad \sigma_g = \frac{\theta_g}{\theta_s} \tag{1}$$

where

$$\theta_s = \frac{2\pi}{S}; \quad \theta_p = \frac{2\pi}{p}. \tag{2}$$

The parameters, thus, that have to be optimized to minimize the cogging torque are given in matrix-format by $\mathbf{X}_1$ in (3). The other machine dimensions to be optimized are given by $\mathbf{X}_2$ in

$$\mathbf{X_1} = \begin{bmatrix} \sigma_m \\ \sigma_t \\ \sigma_g \\ h_r \\ h_s \end{bmatrix}; \quad \mathbf{X_2} = \begin{bmatrix} d_o \\ d_i \\ \ell \\ h_m \end{bmatrix}; \quad \mathbf{U} = \begin{bmatrix} \tau_{ave} \\ \Delta\tau \\ \Delta\tau_L \\ \mathrm{THD} \end{bmatrix}. \tag{3}$$

The performance parameters in $\mathbf{U}$ of (3) are calculated in per unit values as

$$\tau_{ave} = \frac{T_{ave}}{T_{rated}}; \quad \Delta\tau = \frac{\Delta T_{cog}}{T_{rated}}; \quad \Delta\tau_L = \frac{\Delta T_L}{T_{rated}} \tag{4}$$

$$\mathrm{THD} = \frac{\sqrt{\sum_{k=2}^{n} V_k^2}}{V_{1peak}}. \tag{5}$$

$T_{rated} = 1000$ Nm from Table I. The voltage quality of the generator is evaluated by calculating the total harmonic distortion (THD) of the open circuit-induced voltage waveform.

III. Design Optimization Method

The design optimization method proposed in the paper is to first optimize $\mathbf{X}_1$ and $\mathbf{X}_2$ of (3) in terms of the average torque performance, τ_{ave}, of the machine and then to optimize $\mathbf{X}_1$ in a second optimization to minimize $\Delta\tau$. In the same way as described in [27], FE analysis together with an optimization algorithm is used to optimize $\mathbf{X}_1$ and $\mathbf{X}_2$, by maximizing the torque per copper losses of the generator subject to a torque constraint of $\tau_{ave} > 1.0$ pu. In this design optimization, the copper loss is set at $P_{cu} = 600$ W according to the cooling capacity of the wind generator. The outer diameter is set at a maximum allowed value of 667 mm and the axial length is limited to a maximum of $\ell = 100$ mm. The outcome of this design optimization according to the parameters of (3) is found to be

$$\mathbf{X_{1(\mathit{T_{ave}})}} = \begin{bmatrix} 0.98 \\ 1.0 \\ 0.53 \\ 14.0 \\ 8.0 \end{bmatrix} \quad \mathbf{X_{2(\mathit{T_{ave}})}} = \begin{bmatrix} 667 \\ 496 \\ 100 \\ 6.0 \end{bmatrix}$$

$$\mathbf{U}_{(T_{ave})} = \begin{bmatrix} 1.13 \\ 0.26 \\ 0.41 \\ 13.67 \end{bmatrix}. \tag{6}$$

It is clear from (6) that the cogging torque is far too high (26%) for the PM wind generator. The cogging torque is calculated by the Maxwell's stress tensor method, and by position-stepping the rotor till a peak-to-peak torque, ΔT_{cog}, is obtained. All results are calculated from magneto static FE solutions. If static solutions are used, transient effects do not influence the cogging torque results.

Also, from (6), it is seen that the load torque ripple $\Delta\tau_L$ is even much higher than $\Delta\tau$, at a value of 0.41 pu. The THD of the no-load-induced voltage waveform in this case is 13.67%. These values for the THD and $\Delta\tau_L$ are unacceptably high.

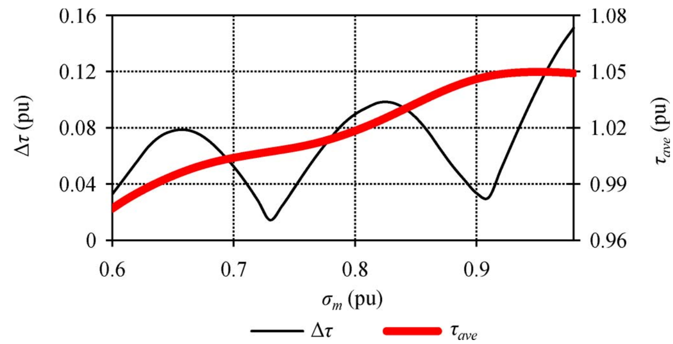

Fig. 4. Per unit cogging torque and average torque versus magnet pitch of the irregular parallel slotted machine [Fig. 2(a)].

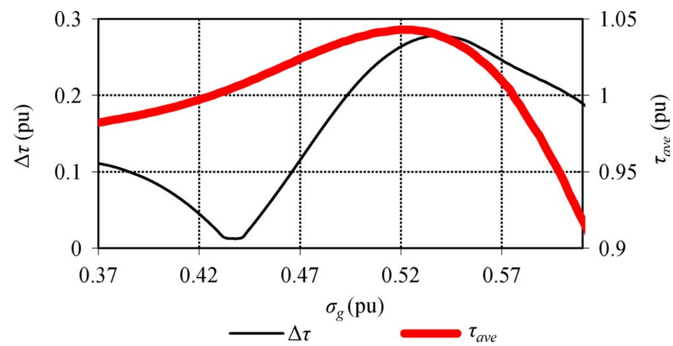

Fig. 5. Per unit cogging torque and average torque versus slot width of the irregular parallel slotted machine [Fig. 2(a)].

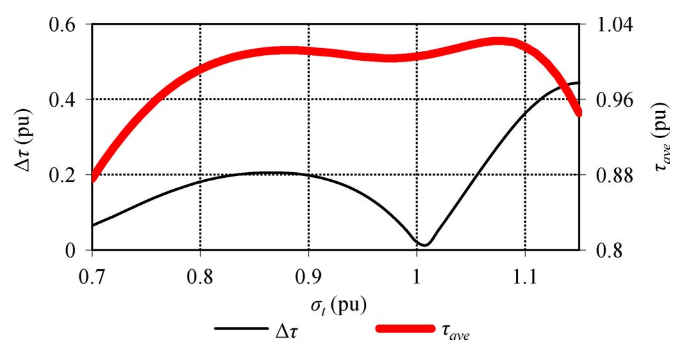

Fig. 6. Per unit cogging torque and average torque versus slot pitch of the irregular parallel slotted machine [Fig. 2(a)].

IV. Effect of Machine Dimensions on Torque

A. Single Parameter Variation

The three parameters in (3) having the largest effect on the cogging torque are σ_m, σ_t, and σ_g. The torque behavior that results from these parameter variations, thus, needs to be thoroughly analyzed. This is done by keeping all machine design parameters and P_{cu} fixed, while varying separately each of the above parameters. The effect of these variations on τ_{ave} and $\Delta\tau$ of the machine of Fig. 2(a) are shown in Figs. 4–6. The much more sensitive nature of $\Delta\tau$ compared to τ_{ave} can be clearly seen. It is clear that the best cogging torque performance occurs at specific values of σ_m, σ_t, and σ_g.

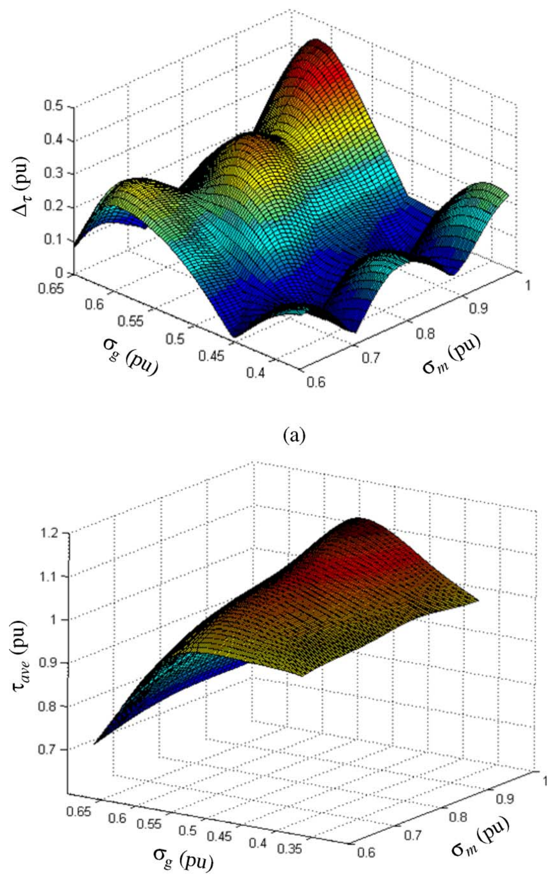

Fig. 7. (a) Per unit cogging torque and (b) average torque versus slot width and magnet pitch of the irregular parallel slotted machine [Fig. 2(a)].

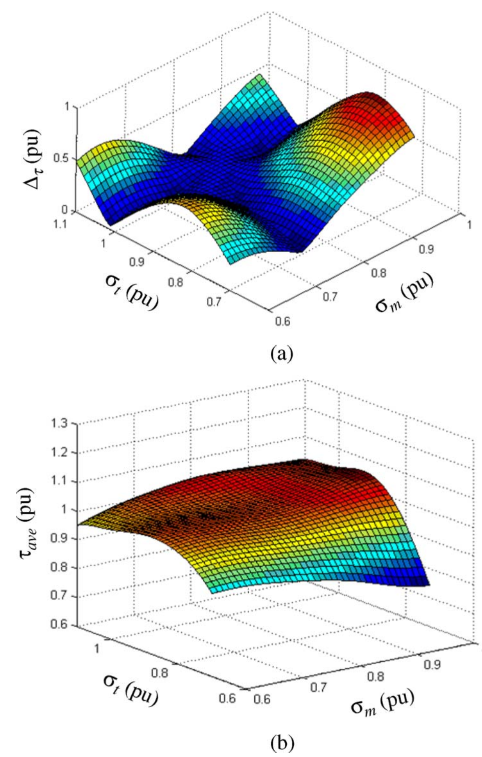

Fig. 8. (a) Per unit cogging torque and (b) average torque versus slot pitch and magnet pitch of the irregular parallel slotted machine [Fig. 2(a)].

Due to the much smaller effect on τ_{ave}, these parameter values can be chosen as the optimum design parameters without affecting the overall machine performance significantly. Note that for all variations h_r and h_s are fixed at $h_r = 7.25$ mm and $h_s = 10$ mm as given in (7).

B. Multi-Parameter Variation

Due to the irregular and sensitive nature of $\Delta\tau$, a more thorough analysis is done through multi-parameter variation with the results shown in Figs. 7–9. A more visualized representation of the machine's torque behavior is obtained in this way. Both Figs. 7 and 8 refer to the irregular parallel slotted machine. To make the effects caused by the irregular slotting clear, Fig. 9 shows the cogging torque results of the regular taper slotted machine.

It is clear that the regular taper slotted machine has a much smoother and overall lower cogging torque than the irregular parallel slotted machine; this is particularly true when comparing Figs. 7(a) and 9(a). However, Figs. 7 and 8 show that low cogging torque values can be obtained for the irregular parallel slotted machine. Again, the smooth and less sensitive nature of the average torque is clear from Figs. 7(b) and 8(b).

Figs. 7–9 give valuable information about the machine's torque behavior and give a clear indication of what parameter values should be chosen. However, to obtain these plots, intensive and time-consuming FE simulations are needed.

To investigate this aspect further, Figs. 10 and 11 shed more light on the optimum parameter regions for best cogging torque performance. Fig. 10 corresponds to Fig. 7(a) where the cogging torque is plotted versus the slot width with the magnet pitch a parameter. Fig. 11 corresponds to Fig. 8(a) where the cogging torque is plotted versus the slot pitch with magnet pitch again a parameter.

It is clear from Figs. 10 and 11 that there are slot-width and slot-pitch regions with an overall low cogging torque, where the cogging torque is very much independent of the magnet pitch. Hence, only these regions need to be investigated more comprehensively. A decent performing machine with low cogging torque can, thus, be obtained, while still staying within acceptable FE simulation times.

C. Effect of Stator and Rotor Yoke Heights

Despite the dominant cogging effects caused by σ_m, σ_t, and σ_g, changes in the stator and rotor yoke heights surprisingly, impose significant cogging torque variations as well. This is shown in Fig. 12, which shows the cogging torque versus the rotor yoke height with the stator yoke height a parameter.

Fig. 13 shows the effect of this variation on the average torque. Again, the sensitive nature of $\Delta\tau$ and the smooth, lesser variation of τ_{ave}, are seen. Note that for $h_s = 10$ mm and $h_s = 13$ mm, almost no change in τ_{ave} is observed in Fig. 13. Also, with this optimization, the reduction in the generator mass can be substantial; it can be seen from Fig. 12 that the lowest

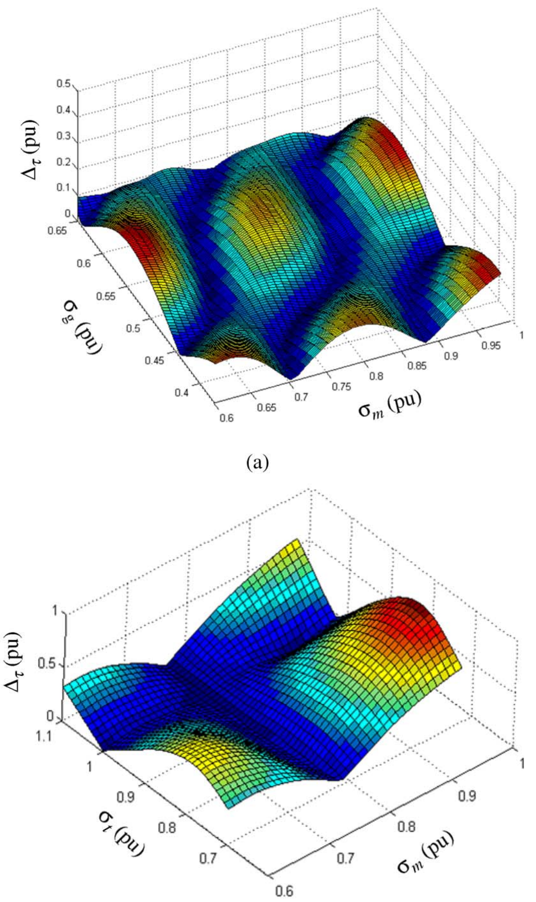

(a)

(b)

Fig. 9. Per unit cogging torque of the regular taper slotted machine [Fig. 2(b)] versus (a) slot width and magnet pitch; (b) slot pitch and magnet pitch.

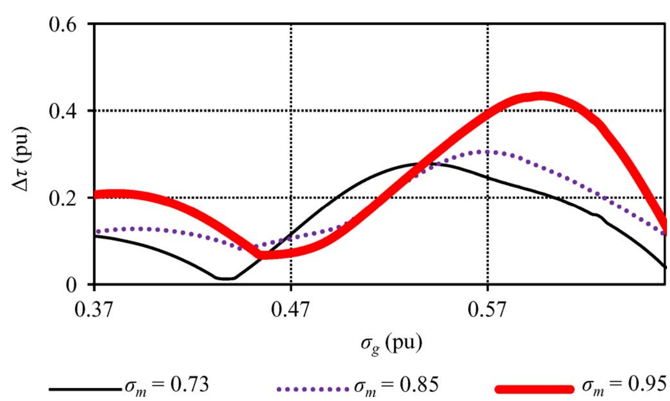

Fig. 10. Per unit cogging torque versus slot width with magnet pitch a parameter of the irregular parallel slotted machine [Fig. 2(a)].

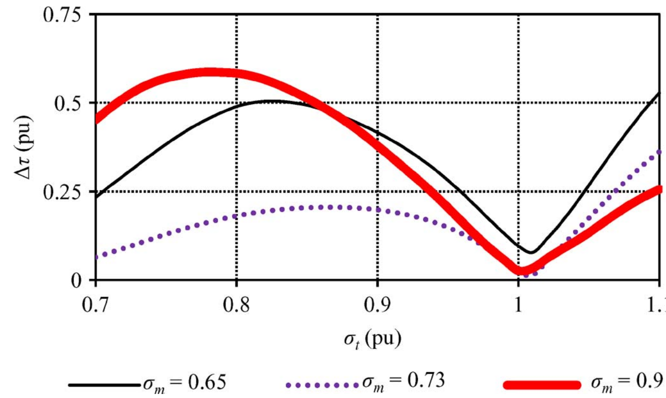

Fig. 11. Per unit cogging torque versus slot pitch with magnet pitch a parameter of the irregular parallel slotted machine [Fig. 2(a)].

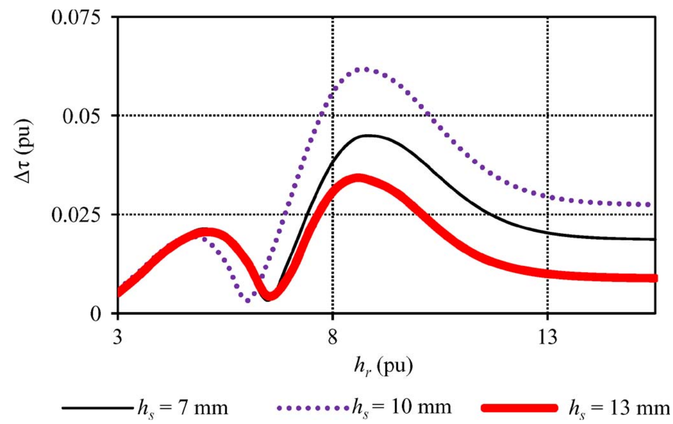

Fig. 12. Per unit cogging torque versus rotor yoke height with stator yoke height a parameter of the irregular parallel slotted machine [Fig. 2(a)].

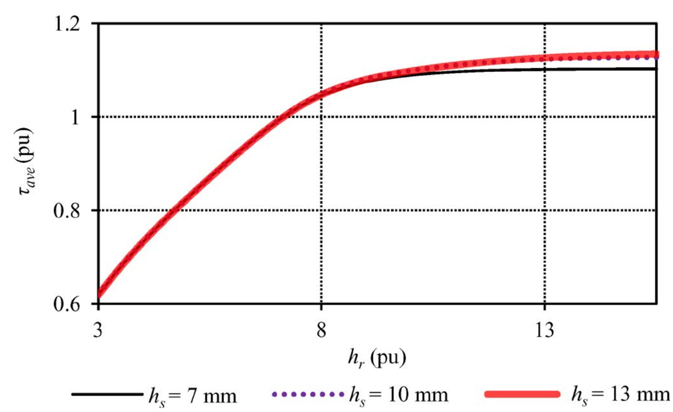

Fig. 13. Per unit average torque versus rotor yoke height with stator yoke height a parameter of the irregular parallel slotted machine [Fig. 2(a)].

cogging torques occur at much thinner rotor yokes than the optimum results of (6).

What is further surprising if Figs. 14 and 15 are observed is that the effects imposed upon $\Delta\tau$ by varying the rotor and stator yokes of the regular tapered slotted machine are almost nothing. This is further confirmed by Fig. 16, which shows the cogging torque of both machine types for a variation in d_i. However, at higher values of d_i, the cogging torque variation of the irregular parallel slotted machine is significantly lower.

The change in cogging torque as the yoke heights are varied might be due to the variation of the reluctance paths, which in turn changes the air gap flux paths of the machine, as parameters are varied. Particularly at the lower rotor yoke heights, saturation in the back-yoke imposes significant effects. Due to the non-uniform spacing at the bottom of the slots caused by the irregular slotting of the machine in Fig. 2(a), the change in yoke height causes the cogging torque to vary considerably. For the regular taper slotted machine of Fig. 2(b), the variation in $\Delta\tau$ is much less due to the uniform changes imposed upon

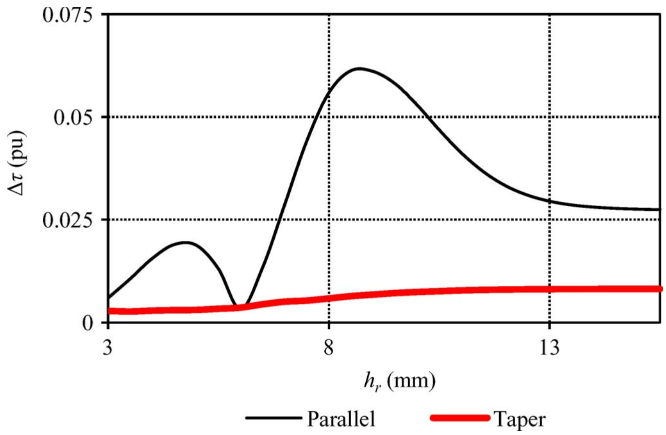

Fig. 14. Per unit cogging torque versus rotor yoke height of the irregular parallel slotted [Fig. 2(a)] and the regular taper slotted [Fig. 2(b)] machines.

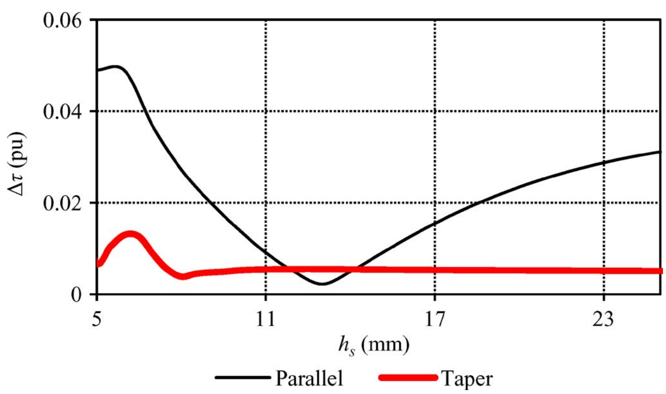

Fig. 15. Per unit cogging torque versus stator yoke height of the irregular parallel slotted [Fig. 2(a)] and the regular taper slotted [Fig. 2(b)] machines.

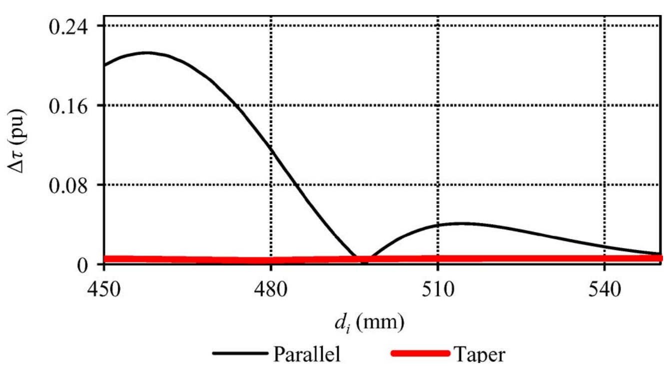

Fig. 16. Per unit cogging torque versus stator inside diameter of the irregular parallel slotted [Fig. 2(a)] and the regular taper slotted [Fig. 2(b)] machines.

the reluctance-flux-paths of the machine if the yoke heights are varied.

Another parameter change investigated is a change in lamination steel. Fig. 17 compares the cogging torque waveforms for two different electrical machine lamination steels. Also, in this case, a clear difference is observed.

D. Selection of Optimum Values

In (7), the optimum parameter values are given for the PM generator that gives the best cogging torque performance. Comparing the performance of the minimum cogging torque design of (7) with the performance of the maximum torque

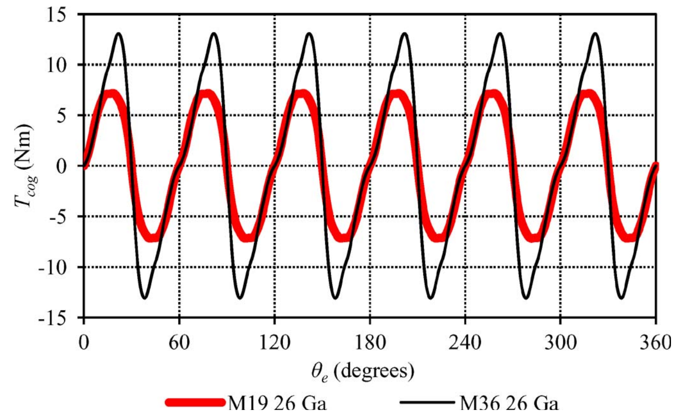

Fig. 17. Cogging torque waveforms of the prototype PM wind generator for two different lamination steels.

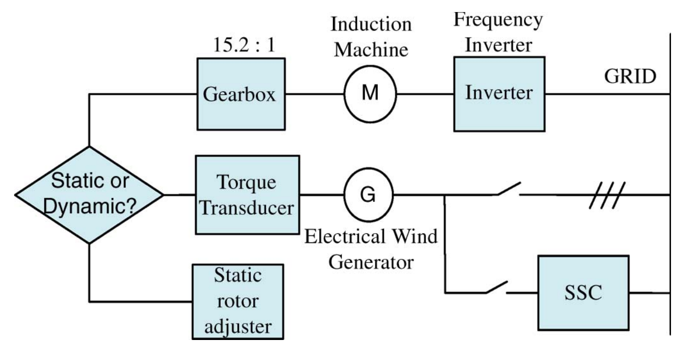

Fig. 18. Diagram of the measurement setup for the PM wind generator.

design of (6), there is a drop in average torque of 13%, but a cogging torque reduction from 26% to 0.2%. Note that the active mass of the design of (7) is also significantly less.

$$\mathbf{X_{1(\Delta\tau)}} = \begin{bmatrix} 0.73 \\ 1.01 \\ 0.44 \\ 7.25 \\ 13.0 \end{bmatrix} \quad \mathbf{X_{2(\Delta\tau)}} = \begin{bmatrix} 653.5 \\ 494 \\ 100 \\ 6.0 \end{bmatrix}$$

$$\mathbf{U}_{(\Delta\tau)} = \begin{bmatrix} 1.00 \\ 0.002 \\ 0.055 \\ 7.14 \end{bmatrix}. \tag{7}$$

V. Torque Ripple Calculation and Measurement

Fig. 18 shows the measurement setup for the prototype PM wind generator. The wind turbine is simulated by an induction motor driven by a frequency inverter to allow for variable speed operation. The motor is connected to the PM generator via a gearbox to reduce the shaft speed to the wind turbine operating speed. The PM generator can be connected directly to the grid or to the grid via the power electronic converter as shown. Furthermore, the induction motor and gearbox can also be disconnected from the system, and the rotor position can be varied in discrete static steps with the torque beam and angle adjuster as depicted in Figs. 19 and 20. When using this static measurement setup, transient effects do not influence the cogging torque results.

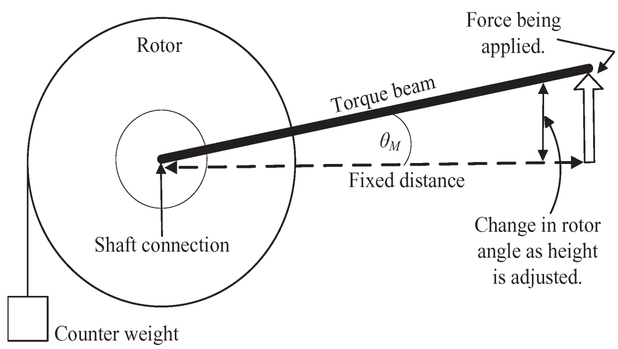

Fig. 19. Diagram of the static cogging torque measurement setup.

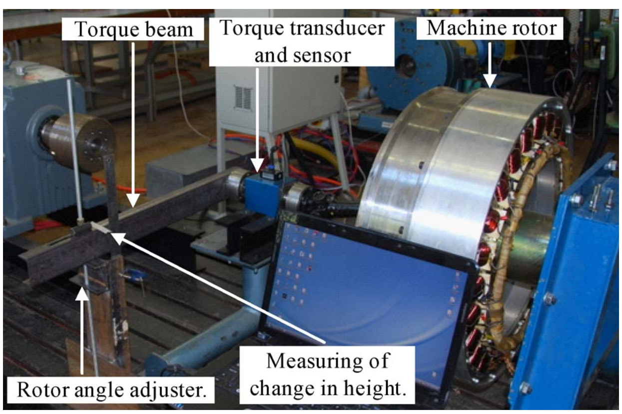

Fig. 20. Static torque measurement setup.

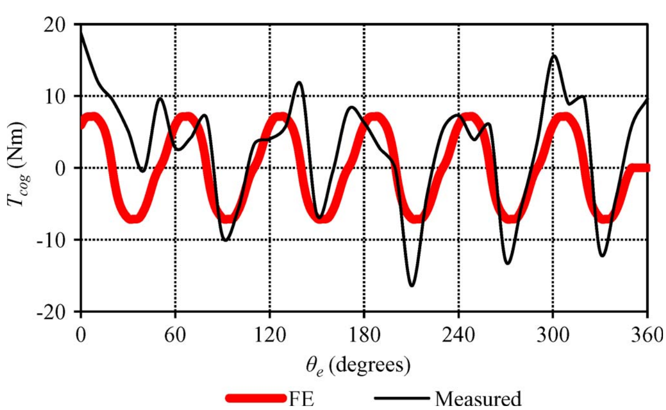

Fig. 21. Measured and FE-calculated cogging torque waveforms of the PM wind generator prototype versus electrical rotor position.

Fig. 19 shows a diagram of the method of cogging torque measurement. Fig. 20 shows the cogging torque measurement setup of the 15-kW PM wind generator prototype. The FE-calculated cogging torque waveform compares well with the measured cogging torque as shown in Fig. 21; note that the design of the prototype generator with a 1.5% no-load torque ripple is not exactly the same as the design of (7). The FE-calculated torque ripple of the prototype generator at rated load is shown in Fig. 22. The load torque ripple is calculated as 4.65%, which is acceptable in terms of torque quality. Due to several dynamic effects within the drive-train test setup, it is not possible to measure this parameter accurately.

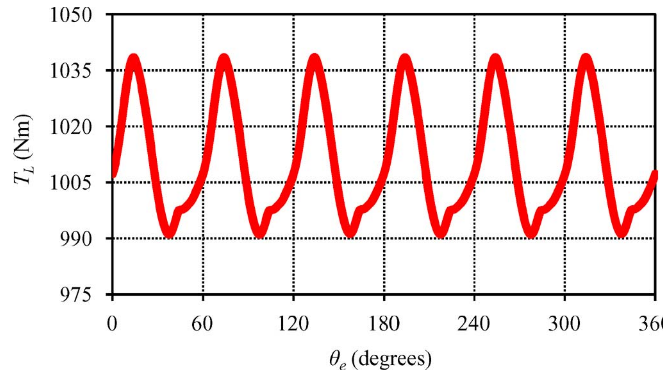

Fig. 22. FE-calculated torque waveform at rated load of the PM wind generator prototype versus electrical rotor position.

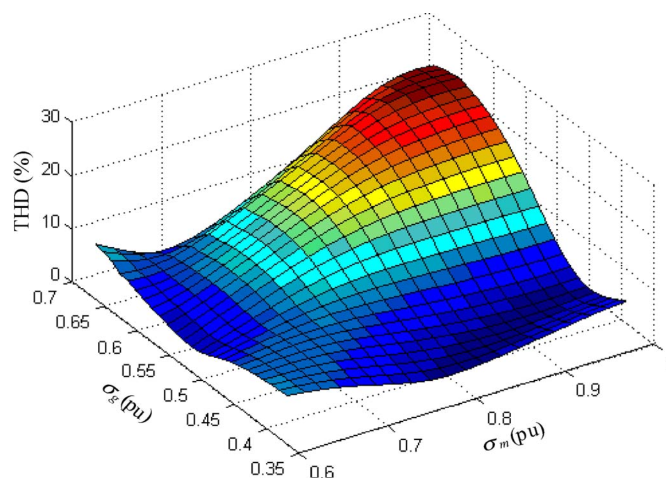

Fig. 23. THD of the no-load-induced voltage versus slot width and magnet pitch.

VI. Voltage Quality

A. Optimizing for the Best THD

In this next section, the possibility of improving the quality of the induced voltage of the single layer winding machine is evaluated. In Figs. 7–9, it is shown that there are regions of low cogging torque. This is also true for the voltage quality of the machine where Fig. 23 shows the THD of the open circuit voltage versus slot width and magnet pitch for the prototype PM generator. Observing Fig. 23, it is seen that there are regions, with an unacceptably high THD as well as regions with a much more acceptable THD. By doing parameter selections within certain regions, it is, thus, possible to also obtain a machine with a low THD as is shown in (8). Comparing (7) and (8), there is a reduction in the THD of 7.14% to 4.64%, but in this case, $\Delta\tau$ and $\Delta\tau_L$ are calculated at 11% and 14%, respectively, which is unacceptable regarding the torque quality of the PM generator

$$\mathbf{X_1}_{(\mathrm{THD})} = \begin{bmatrix} 0.95 \\ 1.01 \\ 0.44 \\ 7.25 \\ 10.0 \end{bmatrix} \quad \mathbf{X_2}_{(\mathrm{THD})} = \begin{bmatrix} 653.5 \\ 494.0 \\ 100.0 \\ 6.00 \end{bmatrix}$$

$$\mathbf{U}_{(\mathrm{THD})} = \begin{bmatrix} 1.02 \\ 0.11 \\ 0.14 \\ 4.64 \end{bmatrix}. \tag{8}$$

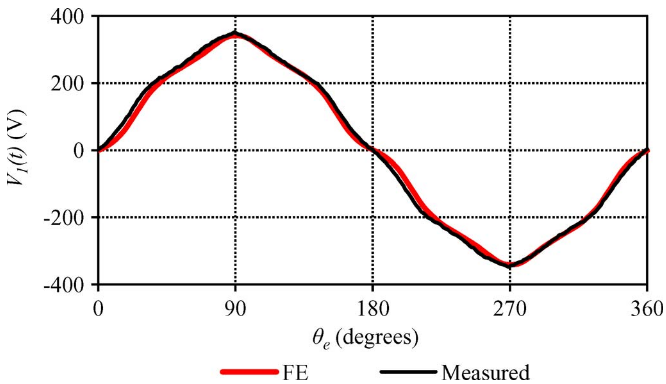

Fig. 24. Measured and FE-calculated per phase no-load voltage waveforms of the wind generator prototype versus electrical angle at 50 Hz.

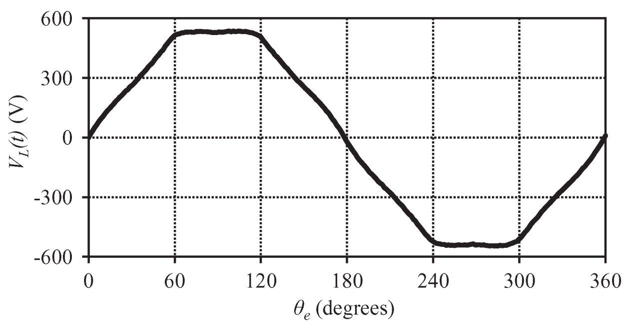

Fig. 25. Measured line voltage waveform versus electrical angle of the wind generator prototype at 50 Hz.

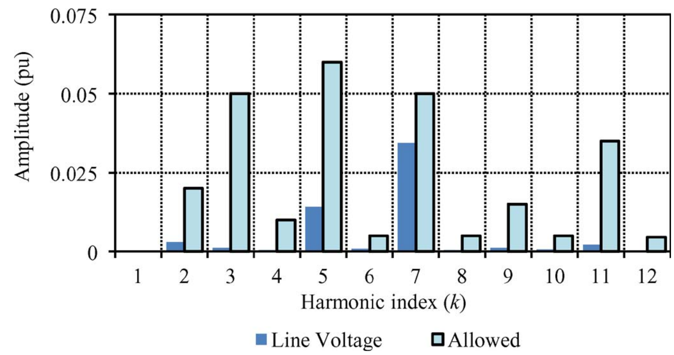

Fig. 26. Harmonic components in the measured line voltage waveform of the prototype PM wind generator, shown with the specifications imposed by the local utility grid.

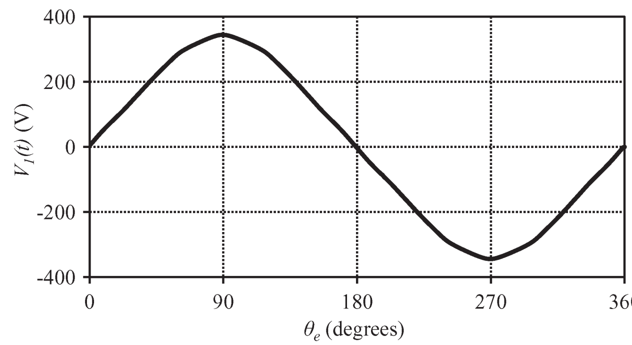

Fig. 27. FE-calculated per phase no-load voltage waveform for a double layer winding PM machine versus electrical angle at 50 Hz.

B. Voltage Waveforms

The FE predicted and the measured per phase voltage of the prototype PM generator are shown in Fig. 24. Fig. 25 shows the measured line voltage. From Figs. 24 and 25, it is clear that there is a significant harmonic content present in the phase and line voltage waveforms. The harmonics present in the line voltage are shown in Fig. 26. Also, shown in Fig. 26 are the requirements imposed by the local utility as stipulated in [31].

From Fig. 26, it is seen that allthough a significant harmonic content is present in the voltage waveforms, the single layer winding waveform still complies with the local utility specifications. The THD of the measured open circuit phase voltage of the prototype PM generator is calculated as 4.3%, which is also much lower than the 8% specified by [31].

Fig. 27 shows the FE-calculated per phase voltage at no-load if a double layer winding is used for the prototype PM generator. A significant improvement is seen, with the distortion of the voltage waveform much less in this case.

VII. Conclusion

A low-cost, low cogging torque PM wind generator with a 10/12 pole-slot combination and parallel open stator slots is proposed and investigated in this paper. It is shown that the average generated torque shows low sensitivity ($\pm 6\%$ of rated torque) to dimension variations in the search for minimum cogging torque. This validates the approach to first do a design optimization based on average values and subject to certain constraints, and then to minimize the cogging torque by final optimization of some of the machine dimensions. The final machine selection should also have an acceptable mass, load torque ripple, and THD.

Minimizing the cogging torque is shown to require a high number of FE solutions to avoid local minimum function values. The minimum cogging torque region, however, can be quickly found by setting the slot pitch equal to 1.0 per unit and by choosing a typical magnet pitch. The per unit slot width region where the cogging torque is a minimum can then be identified. This method is based on the finding that there are low cogging torque regions (valleys) where the cogging torque is fairly independent of the magnet pitch.

An interesting finding is the effect the yoke heights and material type have on the cogging torque. A significant reduction in cogging torque can be obtained by further adjustment of the yoke dimensions. Together with this is the finding that the irregular, parallel slotted layout has in general a higher cogging torque than the regular taper slotted layout. All these results clearly indicate that magnetic saturation in the back iron parts has a significant effect on the cogging torque of the parallel slotted machine.

With regard to manufacturing and assembly tolerances, it is very important in the minimizing of the cogging torque to optimize the dimensions in regions where there is low sensitivity to magnet pitch variations. It is much more difficult to maintain high manufacturing accuracy in the magnet dimensions and placing of the magnets, than in the manufacturing accuracy of the lamination dimensions. Even slight parameter variations due to manufacturing can change the cogging torque significantly.

Regarding the voltage quality of the machine, it is seen that the single layer winding imposes a significant harmonic content in the machine as opposed to the double layer winding. However, it is seen that this harmonic content is still acceptable in the context of [31] and should also be fine for a converter-fed system. It is also seen that the harmonic content can be reduced by doing a similar analysis as for the cogging torque. It is not possible in all cases to achieve selections, which result in an optimum for all output parameters. In this case, cogging torque is identified as the most important output performance parameter.

REFERENCES

[1] N. Bianchi and S. Bolognani, "Design techniques for reducing the cogging torque in surface-mounted PM motors," *IEEE Trans. Ind. Appl.*, vol. 38, no. 5, pp. 1259–1265, Sep./Oct. 2002.

[2] W. Fei and P. C. K. Luk, "Torque ripple reduction of axial flux permanent magnet synchronous machine with segmented and laminated stator," *IEEE Trans. Magn.*, vol. 45, no. 10, pp. 132–138, Oct. 2009.

[3] M. Aydin, Z. Q. Zhu, T. A. Lipo, and D. Howe, "Minimization of cogging torque in axial-flux permanent-magnet machines: Design concepts," *IEEE Trans. Magn.*, vol. 43, no. 9, pp. 3614–3622, Sep. 2007.

[4] M. S. Islam, S. Mir, and T. Sebastian, "Issues in reducing the cogging torque of mass-produced permanent-magnet brushless DC motor," *IEEE Trans. Ind. Appl.*, vol. 40, no. 3, pp. 813–820, May/Jun. 2004.

[5] P. Salminen, J. Pyrhönen, F. Libert, and J. Soulard, "Torque ripple of permanent magnet machines with concentrated windings," presented at the XII Int. Symp. Electromagnetic Fields Mechatronics, Electrical Electronic Engineering (ISEF), Baiona, Spain, 2005.

[6] C. C. Hwang, M. H. Wu, and S. P. Cheng, "Influence of pole and slot combinations on cogging torque in fractional slot PM motors," *J. Magn. Magn. Mater.*, vol. 304, no. 1, pp. e430–e432, Sep. 2006.

[7] Z. Q. Zhu and D. Howe, "Influence of design parameters on cogging torque in permanent magnet machines," *IEEE Trans. Energy Convers.*, vol. 15, no. 4, pp. 407–412, Dec. 2000.

[8] S. A. Saied, K. Abbaszadeh, S. Hemmati, and M. Fadaie, "A new approach to cogging torque reduction in surface-mounted permanent-magnet motors," *Eur. J. Sci. Res.*, vol. 26, no. 4, pp. 499–509, 2009.

[9] L. Gasparin, A. Cernigoj, S. Markic, and R. Fiser, "Prediction of cogging torque level in PM motors due to assembly tolerances in mass-production," *COMPEL: Int. J. Comput. Math. Elect. Electron. Eng.*, vol. 27, no. 4, pp. 911–918, 2008.

[10] S. Rojas, M. A. Pérez, J. Rodríguez, and H. Zelaya, "Torque ripple modeling of a permanent magnet synchronous motor," in *Proc. IEEE ICIT*, Viña del Mar, Chile, Mar. 14–17, 2010, pp. 433–438.

[11] A. G. Yepes, F. D. Freijedo, P. Fernandez-Comesana, J. Malvar, O. Lopez, and J. Doval-Gandoy, "Torque ripple minimization in surface-mounted PM drives by means of PI + multi-resonant controller in synchronous reference frame," in *Proc. 36th IEEE IECON*, Phoenix, AZ, Nov. 7–10, 2010, pp. 1017–1022.

[12] S. Mariethoz, A. Domahidi, and M. Morari, "A model predictive control scheme with torque ripple mitigation for permanent magnet motors," in *Proc. 35th IEEE IECON*, Porto, Portugal, Nov. 3–5, 2009, pp. 985–990.

[13] P. A. Cassani, Z. Peng, and S. S. Williamson, "A novel voltage-profiling method to minimize torque ripples in srm based vehicle propulsion systems," in *Proc. 34th IEEE IECON*, Orlando, FL, Nov. 10–13, 2008, pp. 1089–1094.

[14] Z. Jabbour, A. Riwan, S. Moreau, J. van Rhijn, and G. Champenois, "Identification and compensation of torque ripples of a PMSM in a haptic context," in *Proc. 36th IEEE IECON*, Phoenix, AZ, Nov. 7–10, 2010, pp. 1665–1670.

[15] N. A. Orlando, M. Liserre, V. G. Monopoli, and A. Dell'Aquila, "Speed sensorless control of a PMSG for small wind turbine systems," in *Proc. IEEE ISIE*, Seoul, Korea, Jul. 5–8, 2009, pp. 1540–1545.

[16] J. Beerten, J. Verveckken, and J. Driesen, "Predictive direct torque control for flux and torque ripple reduction," *IEEE Trans. Ind. Electron.*, vol. 57, no. 1, pp. 404–412, Jan. 2010.

[17] D.-H. Lee, J. Liang, Z.-G. Lee, and J.-W. Ahn, "A simple nonlinear logical torque sharing function for low-torque ripple SR drive," *IEEE Trans. Ind. Electron.*, vol. 56, no. 8, pp. 3021–3028, Aug. 2009.

[18] K. Kurihara, T. Kubota, and M. Hori, "Steady-state and transient performance analysis for a single-phase capacitor-run permanent-magnet motor with skewed rotor slots," *IEEE Trans. Ind. Electron.*, vol. 57, no. 1, pp. 44–51, Jan. 2010.

[19] W. Qian, S. K. Panda, and J.-X. Xu, "Torque ripple minimization in PM synchronous motors using iterative learning control," *IEEE Trans. Power Electron.*, vol. 19, no. 2, pp. 272–279, Mar. 2004.

[20] A. Rolan, A. Luna, G. Vazquez, D. Aguilar, and G. Azevedo, "Modeling of a variable speed wind turbine with a Permanent Magnet Synchronous Generator," in *Proc. IEEE ISIE*, Seoul, Korea, Jul. 5–8, 2009, pp. 734–739.

[21] S. M. R. Kazmi, H. Goto, H.-J. Guo, and O. Ichinokura, "A novel algorithm for fast and efficient speed-sensorless maximum power point tracking in wind energy conversion systems," *IEEE Trans. Ind. Electron.*, vol. 58, no. 1, pp. 29–36, Jan. 2011.

[22] B. Beltran, T. Ahmed-Ali, and M. Benbouzid, "High-order sliding-mode control of variable-speed wind turbines," *IEEE Trans. Ind. Electron.*, vol. 56, no. 9, pp. 3314–3321, Sep. 2009.

[23] A. J. G. Westlake, J. R. Bumby, and E. Spooner, "Damping the power angle oscillations of a permanent-magnet synchronous generator with particular reference to wind turbine applications," *Proc. Inst. Elect. Eng.—Elect. Power Appl.*, vol. 143, no. 3, pp. 269–280, May 1996.

[24] H. Müller, M. Pöller, A. Basteck, M. Tilscher, and J. Pfister, "Compatibility of variable speed wind turbines with directly coupled synchronous generator and hydro dynamically controlled gearbox," in *Proc. 6th Int. Workshop Large-Scale Integr. Wind Power Transm. Netw. Offshore Wind Farms*, Delft, The Netherlands, Oct. 26–28, 2006.

[25] S. Grabic, N. Celanovic, and V. A. Katic, "Permanent magnet synchronous generator cascade for wind turbine application," *IEEE Trans. Power Electron.*, vol. 23, no. 3, pp. 1136–1142, May 2008.

[26] J. H. J. Potgieter and M. J. Kamper, "Design of new concept permanent magnet induction wind generator," in *Proc. IEEE ECCE*, Atlanta, GA, Sep. 12–16, 2010, pp. 2403–2408.

[27] M. J. Kamper, F. S. van der Merwe, and S. Williamson, "Direct finite element design optimisation of the cageless reluctance synchronous machine," *IEEE Trans. Energy Convers.*, vol. 11, no. 3, pp. 547–553, Sep. 1996.

[28] D. A. Wills and M. J. Kamper, "Reducing rotor eddy current losses using partial magnet and rotor yoke segmentation," in *Proc. ICEM*, Rome, Italy, Sep. 2010.

[29] S. E. Skaar, O. Krovel, and R. Nilsen, "Distribution, coil-span and winding factors for PM machines with concentrated windings," in *Proc. ICEM*, Sep. 2006, Paper 346.

[30] M. J. Kamper, A. J. Rix, D. A. Wills, and R.-J. Wang, "Formulation, finite-element modelling and winding factors of non-overlap winding permanent magnetmachines," in *Proc.ICEM*, Vilamoura, Portugal, Sep. 2008, pp. 1–5.

[31] Electricity Supply—Quality of Supply, Part 2: Voltage Characteristics, Compatibility Levels, Limits and Assessment Methods, Standards South Africa, NRS 048-2:2004, Jun. 2004.

Johannes H. J. Potgieter (S'10) was born in Oudtshoorn, South Africa, in March 1985. He received the B.Eng. and M.Sc. (Eng.) degrees in electrical and electronic engineering from the University of Stellenbosch, Matieland, South Africa, in 2008 and 2011, respectively. He is currently working toward the Ph.D. (Eng.) degree in the Department of Electrical and Electronic Engineering, University of Stellenbosch.

His current research focuses on wind power generation solutions and the optimizing of permanent magnet machine technologies, including computer-aided design.

Maarten J. Kamper (SM'08) received the M.Sc. (Eng.) and Ph.D. (Eng.) degrees from the University of Stellenbosch, Stellenbosch, South Africa, in 1987 and 1996, respectively.

He has been with the academic staff of the Department of Electrical and Electronic Engineering, University of Stellenbosch, since 1989, where he is currently a Professor of electrical machines and drives. His research interests include computer-aided design and control of reluctance, permanent magnet and induction machine drives.

Prof. Kamper is a South African National Research Foundation Supported Scientist and a Registered Professional Engineer in South Africa.